Damage studies in heterogeneous aluminium alloys using X-ray tomography

J. Gammage, David Wilkinson, J. Embury, Eric Maire

Damage studies in heterogeneous aluminium alloys using X-ray tomography

J. J. GAMMAGE†, D. S. WILKINSON*†,
J. D. EMBURY† and E. MAIRE‡

†Department of Materials Science and Engineering, McMaster University, Hamilton, Ontario L8S 4L7, Canada
‡GEMPPM, INSA de Lyon, Villeurbanne, France

The role of damage on the mechanical response of a heterogeneous material was investigated through X-ray tomography combined with *in situ* tensile deformation. This technique enables one to follow the same population of damage-nucleating particles throughout a tensile test. The results indicate that heterogeneity in the spatial distribution of particles does influence the damage process. In particular, particles that are in clusters tend to nucleate damage at lower strain than isolated particles. Nucleation is also enhanced for larger particles and those with higher aspect ratios. Increasing the number of neighbours around a non-isolated particle has no additional influence on the evolution of damage. A model accounting for the multiple cracking of the second phase particles has been developed and incorporated into a self-consistent effective medium analysis model that includes the final stage of damage linkage between cracked particles. The results suggest that while multiple cracking of particles during deformation does accelerate the loss of work hardening with flow, the linkage of damage is the dominant feature which controls the final ductility.

1. Introduction

In previous studies [1], the reduced ductility of heterogeneous materials containing a stiff, reinforcing second phase has been attributed to premature nucleation and accumulation of damage. The damage mechanisms depend on a number of factors such as interfacial strength, particle volume fraction, shape, size and distribution. The effects of these are often interrelated and understanding how they influence damage processes, and how they are affected by the flow properties of the matrix, will provide insight into ways of increasing the ductility of such dual phase systems.

Investigation of damage in the form of particle cracking has been rather limited, primarily due to the experimental difficulty in observing the damage process. Particle fracture is an inherently stochastic process related to the nature of brittle fracture, making the process difficult both to observe experimentally and to model (at least at

*Corresponding author. Email: wilkinso@mcmaster.ca

the level of individual particles). In addition, the heterogeneous distribution of the second phase in materials like the AA6111/Al_2O_3 composite used in this work complicate the monitoring of damage using conventional techniques because, as will be shown, the distribution influences the strains at which damage nucleates and coalesces.

This work is aimed at providing experimental data that can be used to obtain a clear description of the damage process in this class of materials. Routine tensile testing forms the basis for most studies of mechanical behaviour and this was used here also. However, in composite systems one also needs to know the properties of the matrix alone. This can be obtained directly from the composite, using instrumented indentation testing from which the elastoplastic response of the matrix can be determined.

Quantification of damage itself and its relationship to the overall deformation history was obtained using X-ray tomography coupled with *in situ* tensile testing. This has proven to be a powerful technique for studying damage processes occurring at both the local and global scales. In this study we have been able to quantify the evolution of damage including multiple cracking of particles and the influence of heterogeneity in the particle distribution on the damage processes. The experiments also provided statistical information relating the evolution of damage inside a solid to the overall level of stress and strain.

2. Experimental material

An AA6111 aluminium alloy reinforced with a 4 vol. % Al_2O_3 particles was used in this study. Large Al_2O_3 particles, with diameters in the 30–50 μm range, were used to promote damage through particle fracture and to better enable the study of particle damage. (The latter is related to the 1–2 μm resolution limit of X-ray tomography).

Composite manufacture involved a three-stage process. The first consisted of adding the specified volume fraction of Al_2O_3 to a molten bath of the Al alloy, followed by impulse atomization (Henein). This process produces composite granules from 200 to 500 μm in diameter. These were then hot-pressed to consolidate the material into a billet, roughly a unit cylinder with a diameter of 25 mm. These billets were then hot-extruded both to break up the oxide layers present between the consolidated composite granules and to provide a suitable shape for test samples.

High melt temperatures in the 1200°C range were required to provide adequate wetting of the Al_2O_3 particles in the AA6111 bath. As a consequence the fraction of Mg in the AA6111 was depleted by about an order of magnitude and the Al_2O_3 particles underwent a phase transformation from the initial γ phase to the α form. An in-depth study of both the Mg depletion and the Al_2O_3 phase transformation is provided elsewhere [2]. However, both processes degraded the mechanical properties of the composite.

Establishing the matrix mechanical properties that are required for modelling composite behaviour is challenging because of the varying composition of the alloy following fabrication. Rather than attempt to make unreinforced alloys of the same composition as the matrix in each composite, we have employed a technique utilizing instrumented sharp indentation to estimate the matrix response. To date this

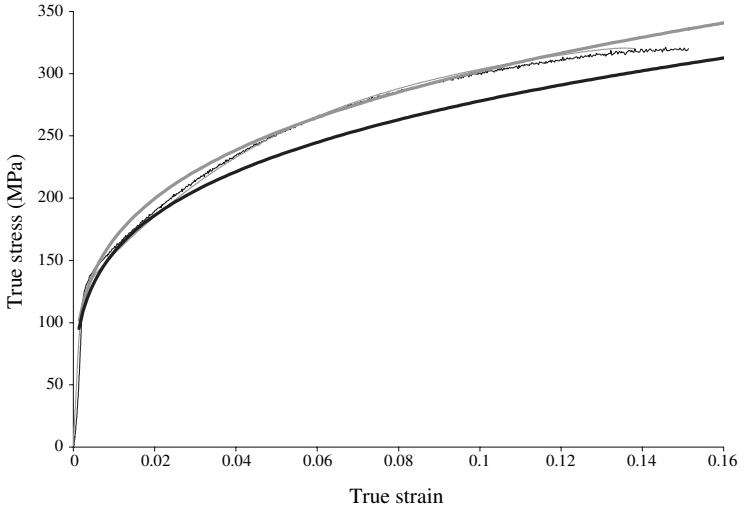

Figure 1. Comparison of the experimental and instrumented sharp indentation predictions of the matrix flow response of two monolithic alloys manufactured via the same process used to manufacture the composite studied in this work. Sample 1. grey (thick predicted-thin experimental). Sample 2. black lines (thick predicted-thin experimental).

technique has been limited to the study of homogeneous materials (e.g. thin films on substrates) [3], and has yet to be tested on composite microstructures. However, Dao *et al.*'s methodology [3] can be applied to extract the stress-strain behaviour of bulk materials or of regions within bulk materials. We have tested this using two homogenous alloys in the present study. Our results, shown in figure 1, are in reasonably good agreement with uniaxial testing data, which gives confidence that the method can be applied as we have done here. In the 4% Al_2O_3 composite studied in this work the technique yielded predictions of a matrix yield strength of 48.8 ± 2.1 MPa and a work hardening exponent of 0.307 ± 0.008.

3. High resolution X-ray tomography

The evolution of damage during tensile deformation was monitored using high resolution X-ray tomography coupled with an *in situ* tensile loading stage [4]. Tomography offers several key advantages over other damage monitoring techniques. In particular, this is a bulk method in which damage is monitored over the total volume and not just the sample surface. Moreover, when coupled with *in situ* deformation, the same particle field is used to study damage evolution over a range of strains. This is not possible using metallographic observations.

X-ray tomography work was conducted at the European Synchrotron Radiation Facility (ESRF) on Beamline ID19. A full explanation of the facilities and the experimental technique employed to produce images with 1–2 μm resolution is described by Maire *et al.* [5] and will only be outlined here for clarity. Two of the key characteristics that provide the resolution capability at ID 19 are the large source-to-sample distance

and the highly collimated, high-energy nature of the X-ray source. A set of radiographs of the same sample is first recorded for different viewing angles. These radiographs are then used as an input for an appropriate software to reconstruct the three dimensional map of the attenuation coefficient in the sample. This absorption gives an indirect image of the microstructure. *In-situ* tensile loading was accomplished via a high precision screw driven loading frame that transmits load from the top portion of the loading machine to the bottom through an (X-ray transparent) polymer tube. During the tests samples were deformed by a predetermined strain following which the test was halted and a tomographic image was taken (keeping the sample under load). This process was repeated several times during each test.

Both qualitative and quantitative data were generated from the raw tomography data files. Thresholding techniques, in this case a region-growing algorithm used in the image processing software VgStudiomax™, enabled segmenting the particles from the matrix. Following this, a second image processing program (called AI3D†) was employed to perform extract statistical information on particle and damage distributions at each of the strain increments.

The calculation of true stress and true strain for the *in situ* tests involved coupling data from the tensile load controller with the tomographic images. The latter were used to determine the current cross-sectional areas A at all load increments including the initial unloaded state, A_o. On average five measurements of cross-sectional area were taken along the gauge length at each increment. At low strains the standard deviation was low and increased to a maximum of $\pm 0.3\,\mathrm{mm}^2$ at the largest deformation. Following these measurements the true strain at each increment was calculated using $\varepsilon = \ln(A_o/A)$. Likewise the true stress in the composite was calculated from $\sigma = P/A$, P being the current applied load. The stress applied to the particles at each increment was estimated from the macroscopic stress using results from the FEM calculations of Brockenbrough and Zok [6]. They found that the stress within hard elastic particles for a uniform distribution of reinforcing particles could be approximated by a stress concentration factor with respect to the macroscopic stress over a wide range of plastic strain and independent of the particle volume fraction. This concentration factor varied from 2 to 2.18, being almost insensitive to volume fraction but somewhat dependent on the work hardening exponent n, with high values of n corresponding to a higher stress concentration. In this work we use a factor of 2.18 since the matrix has a relatively high hardening exponent ($n \sim 0.3$). Moreover, the particle distribution is not uniform. Such heterogeneity in the particle distribution should increase stress partitioning in particle-rich regions which will further increase the stress concentration factor. In the absence of a quantitative analysis of this effect we suggest that using Brockenbrough and Zok's upper limit [6] of $\sigma_p = 2.18\sigma_c$ provides a reasonable estimate of the particle stress.

The dependence of fracture on particle size was also investigated. These results are illustrated in figure 2. After the first increment the average size of the broken particles is considerably higher than that of the full particle field (open circle). As deformation proceeds more of the particles are fractured the average size of the broken

† Developed and kindly provided by Luc Salvo and Charles Josserond, GPM2 Laboratory, INPG, Grenoble.

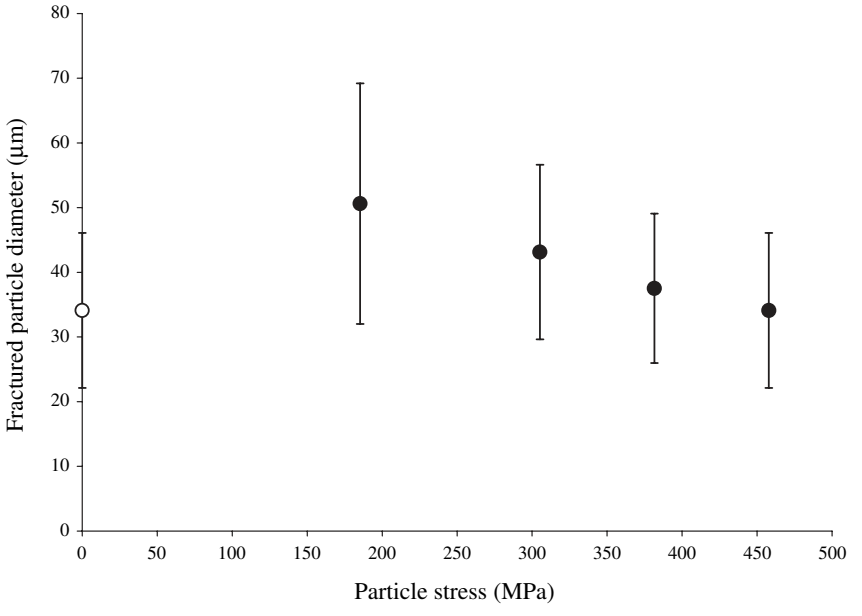

Figure 2. Average and standard deviation of the diameter of fractured particles versus particle stress. Note that at the first loading increment the larger particles fracture first resulting in the highest average cracked particle diameter. As loading continues an increasing number of smaller particles fracture lowering the average cracked particle diameter until it approaches the average diameter of all the particles in the distribution (open circle point at zero stress).

particles starts to fall. It is clear that the largest particles tend to fracture initially. However, there is a large standard deviation to this data (greater than that for the particle size field itself). This may be attributed to the flaw size sensitivity of brittle fracture, whereby those particles that contain the largest defects fracture first. Thus the flaw size distribution, when integrated into the particle size distribution, increases the overall spread of the data. By the final strain increment essentially all the particles are fractured, and so the average and standard deviation of the fractured particle diameter equals that of the undamaged particle distribution prior to loading.

We have also measured the fraction of cracked particles at each strain. This was coupled with the particle stress estimate and fit to the Weibull distribution for brittle fracture (see figure 3). We have found that a two-parameter Weibull analysis (setting the threshold stress equal to zero) best fits the data. The Weibull modulus determined from this analysis is 3.91, which suggests a large variability in the particle fracture strength. This value is consistent with the values of $3 < m < 6$ reported in literature for Al_2O_3 [7] and SiC-reinforced Al–matrix composites [8, 9]. This low value of Weibull modulus is often partially attributed to the polycrystalline nature of the reinforcement and to the manufacturing methods (attrition or spray drying) that result in a wide distribution in internal defect size. It should be noted however that in extracting this data from the tensile tests we assume a uniform particle stress

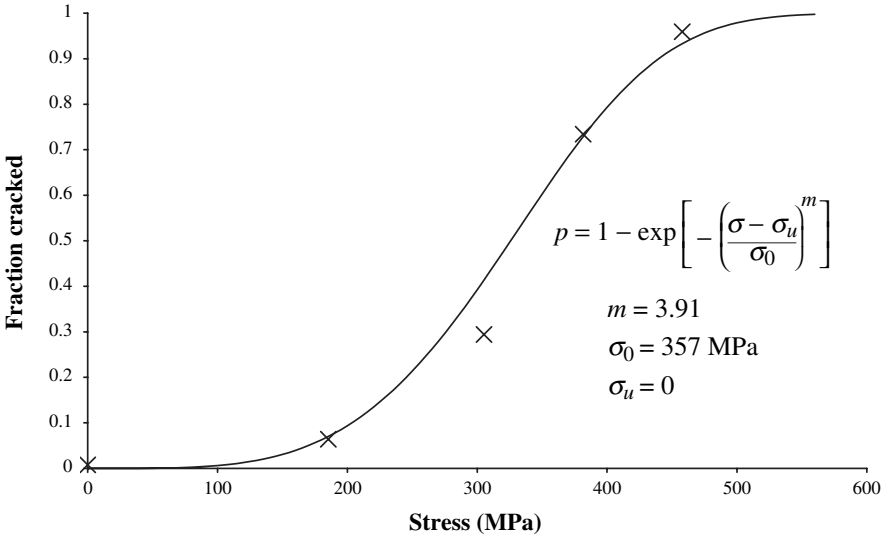

Figure 3. Fraction of cracked particles versus particle stress. Data fit to the Wiebull function for determination of the Wiebull modulus (m), the characteristic stress (σ_0) and the threshold stress (σ_u).

concentration factor. Variability in this factor due to heterogeneity in the spatial distribution of particles helps to lower the Weibull modulus derived in this analysis. The characteristic Weibull strength (a parameter close to but slightly different from the average strength) of the particles is found to be 357 MPa, which is relatively low. This reflects the large particle size since brittle materials lose strength as the stressed volume increases. Moreover, it seems likely that the phase transformation that the particles undergo during processing may introduce flaws that significantly reduce their strength.

A number of features of the damage process were investigated using a 3-dimensional volume viewer on the raw reconstructed tomographic images. This approach makes it possible to follow a set of particles through all the deformation increments. For example, this approach can be used to study the effects of neighbouring particles on damage.

The damage mechanism observed in this material is somewhat atypical, in that most of the particles studied underwent multiple fractures as shown in figure 4. This suggests that the particles remain well-bonded to the matrix thus enabling sufficient further stress partitioning on cracked particles so that they are reloaded up to a new fracture stress. It also reflects the relatively low fracture strength of these particles as determined by the Weibull analysis. Multiple cracking is not generally considered in most composite fracture models [6, 10]. While Zong *et al.* [10] describe the loss of composite stiffness through particle shattering, it is assumed that this occurs instantaneously, not progressively as in the damage process observed in this composite system.

The effect of particle heterogeneity was studied using a multi-step process. Initially, a set of 37 particles were randomly selected. Each of the selected particles

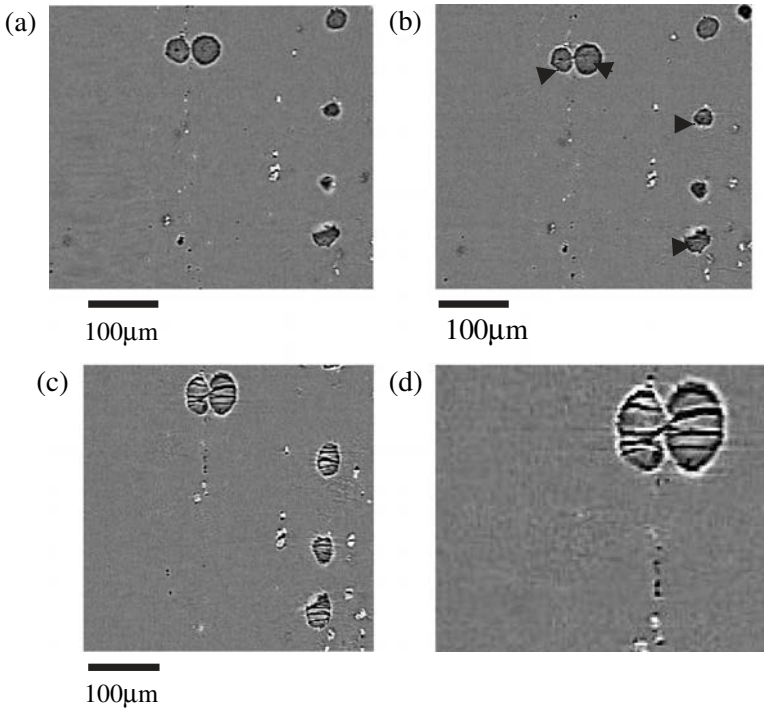

Figure 4. Two-dimensional slices from the three-dimensional volume generated by X-ray tomography. This slice was extracted near the centre of the gauge section. (a) The slice chosen prior to deformation, (b) the same slice at $\varepsilon = 0.098$ and (c) at $\varepsilon = 0.26$ show that many particles are cracked and that the number of cracks per particle increases with strain. Arrows in (b) point to the cracks in the particles. (d) A magnified region of (c) which clearly shows multi-stage cracking.

was then classified based on the number of neighbouring particles surrounding it. Isolated particles were defined as those having no other particles spaced less than one particle diameter away in three dimensions. This was based on published FEM calculations [11, 12] for the distance at which stress fields from neighbouring particles begin to significantly overlap. The non-isolated particles were classified as having one or more neighbouring particles spaced less than or equal to one particle diameter away in any direction, assumed to represent a "region of interest". These particles were then further subdivided as having one, two, three or four or more neighbouring particles within this region.

Once the initial sets of particles were identified, these same particles were followed through all of the subsequent increments. Those that had decohered rather than fractured were removed from the data set. This reduced the total number of sampled particles by three, to 34.

A total of 12 isolated and 22 non-isolated particles were followed at each strain increment. The average number of cracks per reinforcing particle is plotted as a function of the overall composite tensile strain, separating the isolated from the non-isolated particles in figure 5. In both populations the damage

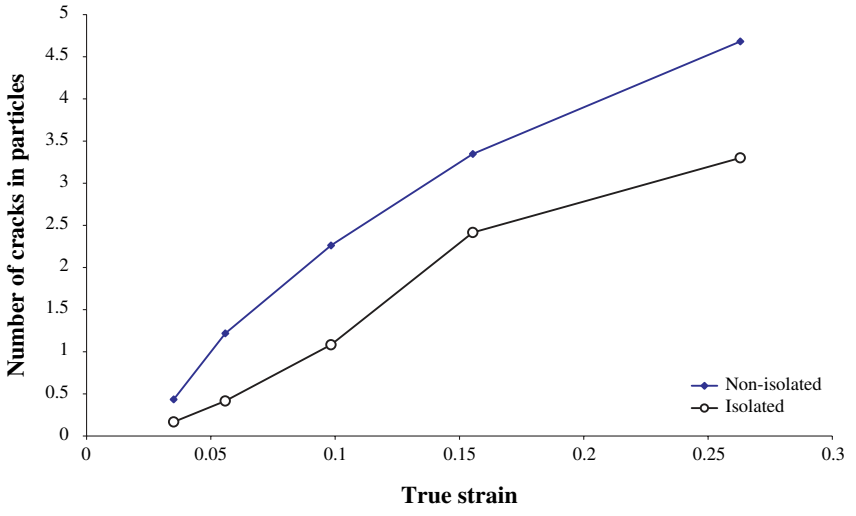

Figure 5. Comparison of the average number of cracks in both isolated and non-isolated particles.

increases more or less linearly with tensile strain. Moreover, at small strain the mean number of cracks for the isolated and non-isolated particles is not significantly different. However, as deformation proceeds, the mean values start to diverge such that non-isolated particles damage more quickly than the isolated particles.

In order to test the significance of this result we have applied the T-test. For two data sets with unequal numbers of data entries T is defined as

$$T = \frac{(\bar{X}_1 - \bar{X}_2) - D_o}{\sqrt{\left(S_1^2/n_1\right) + \left(S_2^2/n_2\right)}}, \tag{1}$$

where X_1 and X_2 are the mean of the isolated particle and non-isolated particle data set respectively. S_1 and S_2 are the standard deviations of each data set and n_1 and n_2 are the number of particles in each set, in this case 12 and 22, respectively. D_0 is the value of the testing hypothesis, where the hypothesis H_0: $\mu_1 - \mu_0 = 0 = D_0$ is used in this work. In this form, the hypothesis states that no difference exists in the mean values of each data set. This hypothesis is rejected, i.e. the differences are statistically significant if the calculated value of T is greater than T_α, where α is the significance level. The test uses a 5% significance level (corresponding to a 95% confidence level), at each strain increment to determine if, statistically, isolated particles undergo less damage than particles with close neighbours. The results are presented in table 1. This test demonstrates that the results are statistically different at all but the first increment of strain.

The increased propensity to damage for clustered particles is consistent with a number of models based on both FEM analysis and self-consistent modelling [1, 13].

Table 1. Comparison of the statistical significance of the difference in the number of cracks in isolated and non-isolated particles at each tensile strain increment.

	Average number of cracks		
Strain	T	T_α	Difference significant?
0.044022	1.28422	2.92	No
0.063027	2.93841	2.4	Yes
0.106295	3.57662	1.943	Yes
0.154764	2.75592	1.98	Yes
0.279314	2.01274	1.77	Yes

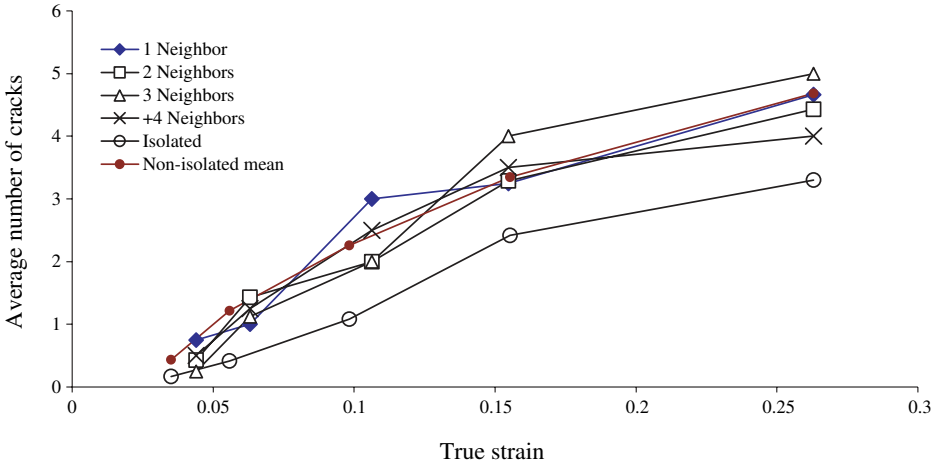

Figure 6. Comparison of the average number of cracks in particles versus tensile strain for particles with 1 neighbour, 2 neighbours, 3 neighbours and 4 or more neighbours. Mean values for the number of cracks in particles for the isolated particles and the entire non-isolated data set are included for comparison.

The simple explanation for this is that particle clustering increases the efficiency of the load shedding process from the matrix to the particles.

The number of cracks per particle was also compared with particles having only one close neighbour, versus those with two, those with three and finally those with four or more neighbours. Each of these subdivided classes only consisted of 5 particles which limits the possible accuracy of this evaluation. However we find that particles with a higher number of neighbouring particles do not seem to contain more cracks than those with fewer neighbours, as shown in figure 6.

4. A model for multiple cracking of particles

The fact that the particles undergo multiple fractures with increased tensile strain suggests that while the particles must unload somewhat after each particle cracking

event, they can be reloaded up to a new level of fracture stress. Based on the flaw size sensitivity of fracture in the ceramic particles, the stress required to produce another crack in the particles must be at least as great as the stress required to cause the preceding cracking event. This has significant implications on the damage process.

The stiffness loss resulting from the multiple cracking of the particles may be considerably higher than that suggested by Brockenbrough and Zok's description [6] of a single fracture event. A description of the multiple cracking process can de developed which makes use of the results from their FEM calculation since it provides a good description of the effect of the loss in particle stiffness when particles fracture. However, the damage parameter derived in Brockenbrough and Zok's work resulted from FEM calculations at fairly low strains ($\sim$1%) since it was found that the strength ratio of the composite flow stress to the matrix flow stress reached an asymptote fairly early in deformation. If the particles are sufficiently strong, reloading the particles up to a new fracture point would be difficult. In this case, the damage parameter derived by Brockenbrough and Zok [6] would be sufficient to describe the loss of stiffness resulting from particle cracking throughout the entire deformation process (excluding the final stage of microcrack linkage). However, when the particle strengths are low, and the modulus mismatch remains high, as in the composite material used in this study, the particles can be subjected to high stress at some distance from the crack plane. It seems reasonable to expect that this additional fracturing of the particles will further reduce the stiffness of the previously fractured particles. We have modelled this by coupling the results of Brockenbrough and Zok's FEM calculation with an estimate of the region within the particle that is still capable of bearing stress.

4.1. *Model development*

Our starting point is an experimental determination of the average number of cracks found in the particles as a function of the tensile strain. The tomography results are shown in figure 7. A linear expression is then fitted to this data giving the average number of cracks per particle, n, as

$$n = 19.2\varepsilon_c \tag{2}$$

where ε_c is the composite tensile strain. We assume that after each cracking event a region of the particle close to the crack is unloaded while the remainder of the particle volume continues to follow the behaviour predicted by the work of Brockenbrough and Zok [6]. The thought process employed to develop the model is outlined schematically in figure 8.

Each crack in the particle unloads an amount of material equal to $V\alpha$ where V is the total particle volume. This fraction of the damaged particle is assumed to have zero stiffness. The remaining material follows the loading behaviour described by Brockenbrough and Zok [6]. Expressions for the fraction of the particle volume that is unloaded and that which follows the Brockenbrough–Zok model

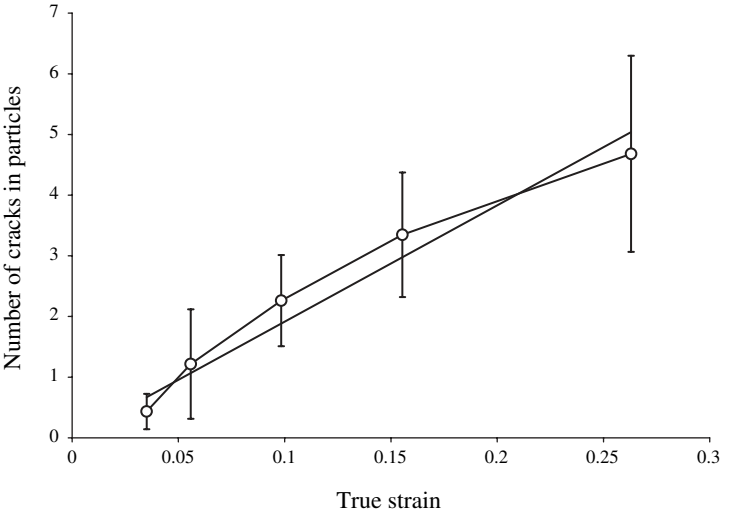

Figure 7. The average number of cracks in cracked particles versus true tensile strain using the full particle field. A linear relationship has been fit to the data, giving a slope of 19.2, passing through the origin.

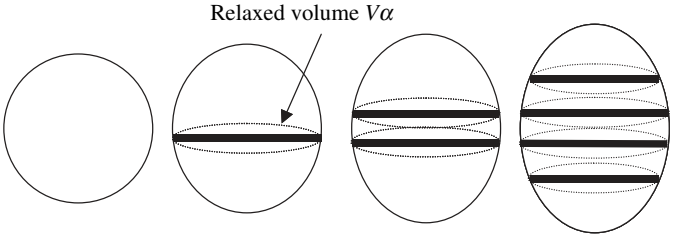

B & Z	V	$V(1-\alpha)$	$V\left(\frac{2}{3}-\alpha\right)$	$V\left(1-2-\frac{n-1}{n+1}\right)$
Unloaded	0	$V\alpha$	$V\left(\alpha+\frac{2}{3}\right)$	$V\left(\alpha+\frac{n-1}{n+1}\right)$

Figure 8. Schematic illustration of the thought process used to develop a damage model incorporating particle multiple cracking. B & Z refers to the volume of material that follows the damage behaviour described by the FEM calculation of Brockenbrough and Zok [6]. Unloaded refers to the volume of fraction of each particle that is completely relaxed following each fracture event.

(defined as "B & Z" in figure 8), can be written for n cracks as

$$V\left(\alpha+\frac{n-1}{n+1}\right) \rightarrow \text{Unloaded Material} \tag{3}$$

$$V\left(\frac{2}{n+1}-\alpha\right) \rightarrow \text{B \& Z Material} \tag{4}$$

where α is a parameter describing the fraction of the particle volume unloaded with each additional crack in the particle.

4.2. *Modelling results*

The model describing the stiffness loss associated with the multiple cracking of the second phase particles has been incorporated into a self-consistent effective medium approximation damage model (SCEMA-Damage). The SCEMA approach uses an iterative algorithm based on calculating the instantaneous work hardening rate (the effective tangent modulus) at each strain increment. It enables one to incorporate a range of microstructural complexity, such as particle clustering, while also providing for a changing relative volume fraction of particles that have linked or cracked. A complete description of this approach is given elsewhere [2, 13, 14]. In this case the stiffness loss associated with particle fracture, described by Brokenbrough and Zok [6], was replaced by that from the multiple cracking model just described. This model was then compared with the original SCEMA-Damage model and evaluated to determine the sensitivity to the value of the unload parameter α and the fit to the experimental data.

The material parameters needed by the model are drawn from our X-ray tomography and instrumented sharp indentation work. The Al_2O_3 particles are assigned a modulus of 390 GPa while the fracture behaviour is described by a Weibull modulus, m, of 3.91 and a characteristic stress, σ_0 of 357 MPa.

The matrix alloy has an elastic modulus of 70 GPa. The elastoplastic response, determined directly from the instrumented sharp indentation results using the method proposed by Dao *et al.* [3] gives

$$\sigma = \begin{cases} E\varepsilon & \text{for } \sigma_y \geq \sigma \\ \sigma_y\left(1 + \dfrac{E}{\sigma_y}\varepsilon_p\right)^n & \text{for } \sigma \geq \sigma_y \end{cases} \tag{5}$$

from which we get $n = 0.307$ and σ_y of 48.8 MPa. This data was then fit to the Ramberg–Osgood power law hardening equation:

$$\varepsilon = \frac{\sigma}{E} + \alpha' \frac{\sigma_o}{E}\left(\frac{\sigma}{\sigma_o}\right)^{1/n} \tag{6}$$

since this is the form of constitutive equation used in the self-consistent model. The value of the scaling parameter, α', and elastic modulus, E, were held constant at 3/7 and 70 GPa, respectively. The value of the work hardening exponent is unchanged, i.e. $n = 0.307$ while the reference stress σ_o is 30 MPa.

Since the matrix flow properties are used directly in the model, the accuracy of the predicted composite response is sensitive to how closely the instrumented microhardness measurements match the flow response of the matrix. The modelling results used in the comparisons that follow should therefore be treated as estimates used to predict the general trends observed in the experimental composite material.

The modelling results, presented in figure 9, predict a slightly stronger response than what is observed experimentally. This is not entirely unexpected since the flow properties of the matrix are overestimated slightly based on the instrumented

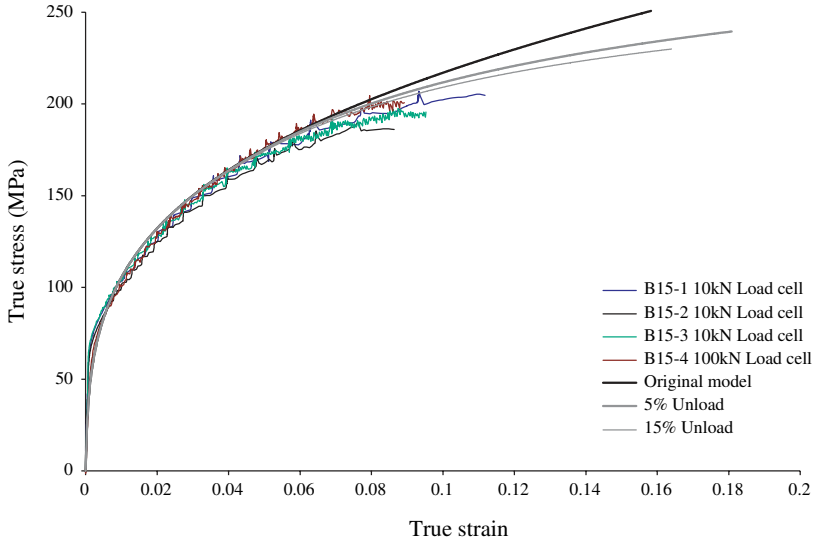

Figure 9. Comparison of experimental and predicted flow curves for the composite containing 4% volume fraction Al_2O_3.

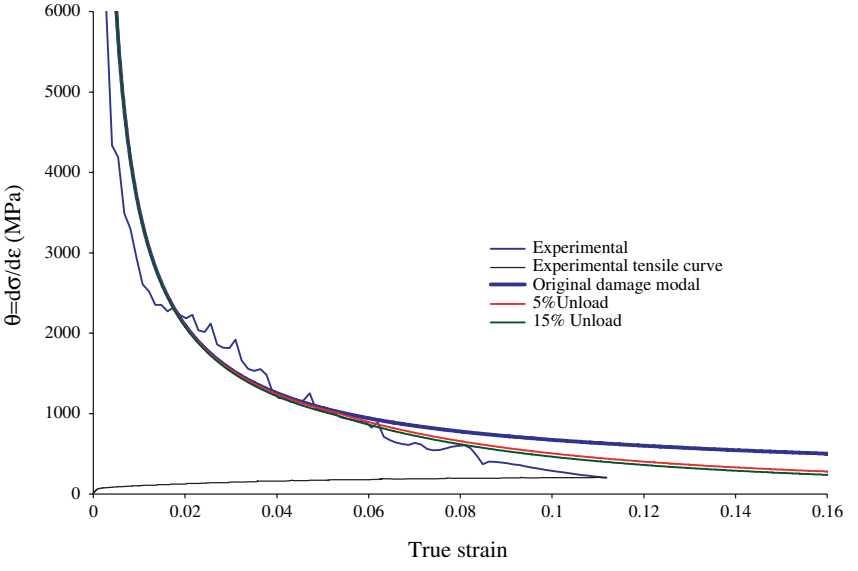

Figure 10. Comparison of the experimental and predicted work hardening rates ($\theta = d\sigma/d\varepsilon$) for the 4% volume fraction Al_2O_3 composite.

micro-hardness measurements, particularly at low strains, as shown in figure 1. Comparison of the predicted and experimental work hardening rates in figure 10 provides a better picture of the role of particle multi-cracking and the significance of the unload parameter α on the composite loading response. At low strains all the

models – including the original SCEMA-Damage model – under-predict the drop in the work hardening rate. At higher plastic strains however, the work hardening rate predictions of the multiple cracking models are closer to the experimental data than those of the original damage model. Qualitatively, higher values of the unload parameter appear to provide better predictions of the composite work hardening rates at high tensile strains, although the results are only weakly dependent on α. Accounting for the additional loss in work hardening associated with particle multiple cracking however fails to capture the point at which failure, as defined by Considère condition, occurs in the experimental material.

4.3. *Incorporating damage linkage into the model*

The particle multiple cracking model provides a better prediction of the experimentally observed deformation behaviour than the original SCEMA-Damage model due to the incorporation of the additional softening resulting from the multiple cracking. However the tensile ductility predictions are still much higher than what is observed experimentally. In order to correct this problem the model must include a coalescence stage. We therefore combine the model just presented with a microcrack linkage model described elsewhere [14]. The latter treats the process of matrix failure in ligaments between damaged particles. This is allowed to occur once the ligament stress exceeds the work hardening rate in the composite. The same input parameters described in the previous section are employed.

The model predicts failure at much lower strain than that based on using the particle multiple cracking model alone – without damage linkage, as shown in figure 11. At these strains the softening attributed to the particle multiple cracking is

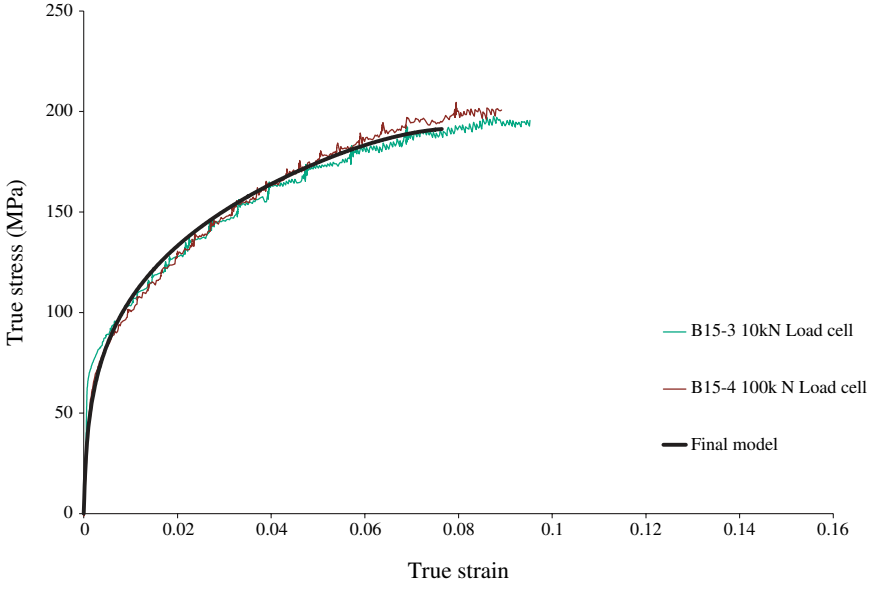

Figure 11. Comparison of the experimental and predicted flow curves resulting from the combined particle multiple cracking and microcrack linkage models for the composite.

small and differences in the predicted flow response for varying values of the unload parameter, α, are negligible. In figure 12 for the work hardening rate one sees clearly that the predictions of failure strain now underestimate the behaviour. This can be attributed to the fact that the linkage model criterion provides a lower bound to the composite ductility [14]. These results suggest that while particle multiple cracking may reduce the composite work hardening at high plastic strains this is not important at the strain levels for which the experimental materials failed. Instead, damage coalescence effectively over-powers these contributions. These results suggest that once damage evolution, measured in terms of the fraction of cracked particles, becomes significant, the linkage of damage through the matrix between adjacent cracked particles will dominate other factors influencing the composite response.

5. Conclusions

X-ray tomography work reveals that damage evolves roughly linearly with strain within the bulk when measured in terms of the fraction of cracked particles or the number of cracks within the multiply cracked particles. Both the largest particles and those with the highest aspect ratio tend to fracture first during deformation. The results also show that damage development during tensile deformation is well described by the Weibull function.

Damage is affected by the spatial distribution of particles such that the amount of tensile deformation required to initiate damage is reduced when particles are in clusters. Once nucleated, damage evolves at roughly the same rate for clustered and

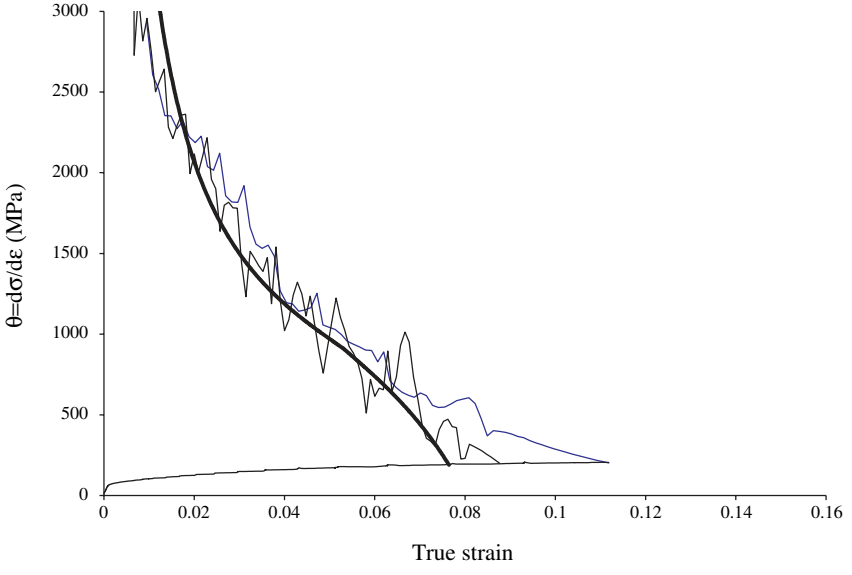

Figure 12. The model prediction of the work hardening rate (thick line) is compared with two experimentally measured work hardening rates (thin jagged lines). The experimentally measured tensile loading curve for one of the samples is included.

isolated particles. The results also show that the damage in non-isolated particles is influenced by the ratio of particle spacing to particle diameter but not by the density of particles contained within a particle-rich region.

A model for deformation incorporating particle multiple cracking predicts a reduction in the work hardening rate above that predicted based on particles undergoing only a single cracking event. This reduction in work hardening however was not significant at the values of strain over which the current experimental material failed. Combining this model with a microcrack linkage model yielded predictions that were in much better agreement with experiment. Once damage, measured in terms of the fraction of cracked particles, becomes significant the linkage of damage through the matrix between adjacent cracked particles will dominate other processes influencing the mechanical response of the composite.

Acknowledgements

The authors are grateful to Prof. Yves Brechet, INPG, France for several fruitful discussions during the course of this research and to Dr. P. Cloetens, ESRF Beamline ID19 for assistance with the tomography experiments. JG acknowledges the financial support of Alcan Intl and NSERC through the provision of graduate scholarships. The authors acknowledge the financial support of NSERC.

References

[1] J. Llorca, in *Comprehensive Composite Materials*, edited by T.W. Clyne (Elsevier, St. Louis, 2000).
[2] J. Gammage, Damage in heterogeneous aluminium alloys, PhD thesis, McMaster University (2002).
[3] M. Dao, N. Chollacoop, K.J. Van Vliet, *et al.*, Acta mater. **49** 3899 (2001).
[4] J.-Y. Buffière, E. Maire, P. Cloetens, *et al.*, Acta metall. **47** 1613 (1999).
[5] E. Maire, J.Y. Buffière, L. Salvo, *et al.*, Adv. Engng. Mater. **3** 539 (2001).
[6] J.R. Brockenbrough and F.W. Zok, Acta metall. mater. **43** 11 (1995).
[7] T. Mochida and M. Taya and D.J. Lloyd, Mater. Trans. Japan Inst. Metals **32** 931 (1991).
[8] Y. Brechet, J.D. Embury, S. Tao, *et al.*, Acta metall. mater. **39** 1781 (1991).
[9] J. Llorca and P. Poza, Acta metall. mater. **43** 3959 (1995).
[10] B.Y. Zong, X.H. Guo and B.L. Derby, Mater. Sci. Technol. **5** 827 (1999).
[11] C. Guillemer-Neel, X. Feauges and M. Clavel, Metall. Mater. Trans. A **31** 3075 (2000).
[12] D.F. Watt, X.Q. Xu and D.J. Lloyd, Acta mater. **44** 789 (1996).
[13] D.S. Wilkinson, E. Maire and R. Fougeres, Mater. Sci. Engng A **262** 264 (1999).
[14] J.J. Gammage, D.S. Wilkinson, J.D. Embury, *et al.*, Acta mater. **54** 5255 (2005).